

GENERALIZATION OF NON-ITERATIVE NUMERICAL METHODS FOR DAMAGE-PLASTIC BEHAVIOUR MODELING

R. GRAÇA-E-COSTA*, J. ALFAIATE†, D. DIAS-DA-COSTA†† AND L. J. SLUYS†††

*ICIST, and Department of Civil Engineering, ISE, Universidade do Algarve,
Campus da Penha, 8000-117, Faro Portugal
Email: rcosta@ualg.pt

† ICIST, and Department of Civil Engineering, Instituto Superior Técnico,
Technical University of Lisbon, Av. Rovisco Pais, 1049-001 Lisbon, Portugal
Email: alfaiate@civil.ist.utl.pt

†† INESC, and Department of Civil Engineering, University of Coimbra
Rua Luís Reis Santos, 3030-788 Coimbra, Portugal
Email: dias-da-costa@dec.uc.pt

††† Department of Civil Engineering and Geosciences, Delft University of Technology,
The Netherlands
Email: l.j.sluis@tudelft.nl

Key words: Non-iterative Energy Based Method, Damage-Plastic Unloading, Discrete Crack Approach, Non-iterative analysis

Abstract: Modelling fracture in concrete or masonry is known to be problematic regarding the robustness of iterative solution procedures and, the use of non-iterative methods (or that minimize the use of iterations) in quasi-brittle materials is now under strong development, due to the necessity to obtain effective results in finite element analysis [1, 2] where strong non-linearities emerge that are otherwise unwieldy to model.

In the proposed lecture, two new methods designated as Non-Iterative Energy based Method (NIEM) and *Automatic* presented in [1, 3] are applied with extension to modelling damage-plastic behaviour. The new methods combine an incremental-total procedure with the preferential use of incremental steps, switching to the total approach only at critical bifurcation points. The development of the load-unloading abilities is allowed by these incremental/total methods, which take advantage of keeping the material's stress/strain memory due to the preferential use of an incremental procedure. A new approach to the unload-load cycles is used in the scope of a non-iterative procedure, which will mitigate the numerical difficulties inherent to cyclic loading.

The formulation for both methods for structures with both softening and hardening behaviour is presented and a structural example where the numerical results are compared with experimental results.

1 INTRODUCTION

The use of total approaches based on a secant stiffness allows for the correct modelling of concrete and masonry structures

under monotonic solicitation [2]. However, in the total approach only secant unloading is assumed (path 4 in Figure 1) and reloading will recover the position on the material envelope using the same secant stiffness. This

is a simplification of the real behaviour, since there is no evaluation of the residual strains or crack openings.

In fact, modelling the behaviour of structures under reversed loading, such as cyclic actions or a load decrease on a given structural member, is not correctly simulated by the secant unloading-reloading (damage) constitutive law; instead, plastic, plastic-damage (Figure 2) or hysteretic laws should be adopted.

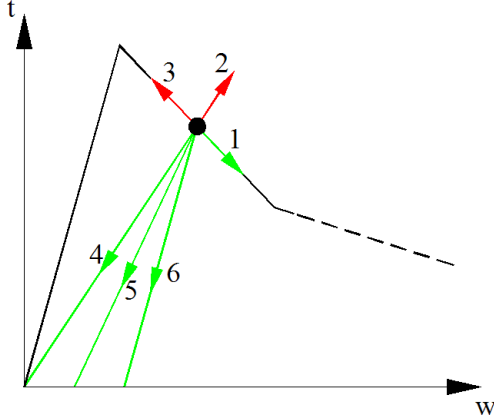


Figure 1: Stress-displacement paths

In Figure 2, 1D representations of the three types of unloading-reloading laws adopted with the new non-iterative methods are presented for softening. In this figure, d refers to an isotropic damage parameter, that easily translates the current stiffness coefficient of any integration point i as a function of the initial elastic stiffness D^e :

$$d_i = 1 - \frac{|t_j|}{D_i^e |w_{j-1} + \Delta w_j|} \quad (1)$$

with,

$$0 \leq d_i \leq 1$$

And is used to define the material stress/strain history. The plastic-damage parameter d_h (Figure 2 c)), is a numerical parameter that takes into account the residual strain/displacement jump ($d_h \leq d$).

The unloading-reloading cycles are approximated with a linear branch, initially defined by the elastic stiffness, with the possibility of evolving according to the plastic-damage d_h function. In the following, D refers

to the tangent constitutive modulus whereas K is the secant modulus.

Experimentally, steel reinforcement exhibits unloading-reloading behaviour which is modelled by means of an elastic branch, since the reinforcing steel is assumed as an elastic-plastic material.

As for concrete, this assumption consists on a simplification in both the compressive and the tensile stress states, since the unloading-reloading cycle is associated with an increase in damage. Under compression, this simplification is possible on low levels of post-peak damage and for slow unloading-reloading cycles, since damage increase also depends on these factors. Another simplification is to substitute the hysteretic cycles by linear elastic-damage branches like the examples in Figure 3.

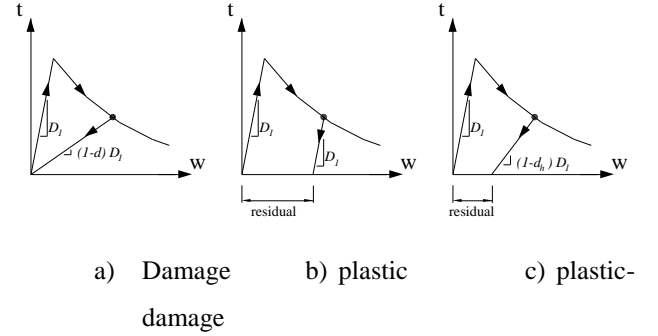


Figure 2: Unloading behaviour

All above referred models, simplified or not, cannot be implemented in a pure total approach. Nevertheless, the introduction of new methods combining an incremental procedure with a total approach opened the possibility of modelling the unloading behaviour taking into account residual deformations.

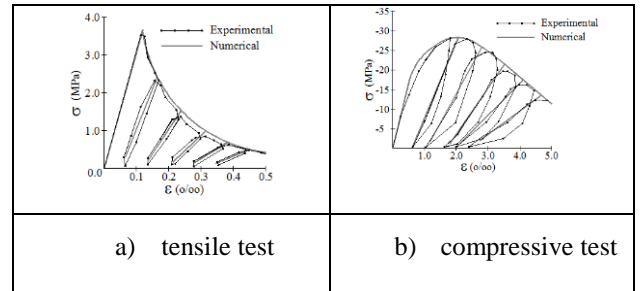


Figure 3: Experimental cyclic loading results and damage branch simplification (adapted from [4])

2 NON-ITERATIVE PROCEDURES

The new non-iterative procedures proposed in [1] use the combined incremental and total approaches. This combined procedure allows for the proper tracking of the material loading history, conversely to purely total methods. Furthermore, information obtained from the previous incremental solution is used to predict the constitutive law adopted in the total approach. In this way: i) there is no need to adjust the material parameters to ensure mesh objectivity; and ii) the consistency condition is satisfied.

2.1 Solution control

In the incremental approach, whenever a bifurcation point is reached, the path choice is based upon the signal of the particular load increment leading to the largest incremental energy dissipation. It is assumed that, for a load increment applied on a structure, the corresponding evolution on the stress-strain law of the material point should follow the path which would release the largest amount of energy. Using an incremental approach, the second order energy release in a finite element, ΔG , is given by:

$$\Delta G = \int_{\Omega} \Delta \boldsymbol{\varepsilon}^T \Delta \boldsymbol{\sigma} d\Omega + \int_{\Gamma_d} \Delta \mathbf{w}^T \Delta \mathbf{t} d\Gamma_d, \quad (2)$$

where Ω is the bulk and Γ_d stands for all discontinuities, $\boldsymbol{\varepsilon}$ and $\boldsymbol{\sigma}$ are the strains and the stresses in the bulk, respectively, and \mathbf{w} and \mathbf{t} are the jump displacements and the tractions, respectively, at the discontinuities.

Since multilinear constitutive relations are adopted, a critical load factor (λ_{crit}) is first evaluated in a trial step, in order to reach the nearest material point connecting two linear branches. Afterwards, the true step is enforced such that:

$$\Delta \mathbf{P}_{true,j} = \lambda_{crit} \Delta \mathbf{P}_{trial,j} \quad (3)$$

2.2 Critical bifurcation points

When bifurcation points are reached on the material law, two possibilities occur: increase of damage or unloading. In Figure 4, four paths on the uniaxial traction-displacement

curve are displayed: path 1 corresponds to increase of damage, paths 2 and 3 are unacceptable since they violate the material law, and path 4 corresponds to secant unloading.

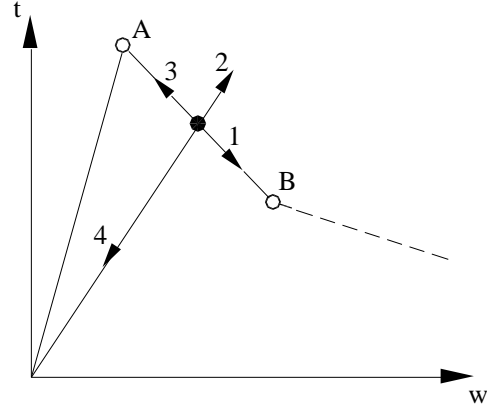


Figure 4: 1D representation of possible traction-jump paths

Whenever a material point undergoes unloading, memory is kept until it reloads back to the envelope. When the current state is unloading this point is never critical except for preventing overlapping of crack faces but, when reloading occurs, the load factor is estimated, similarly to what is done for all points that remain on the envelope. When several nonlinearities arise during the analysis due to the existence of many bifurcation points, path searching techniques must be applied. If no solution is obtained, *i.e.*, if no single admissible path is obtained, a transition to the total approach is made. This aspect is common to both methods herein presented.

2.3 Automatic method

In the *automatic* method, whenever a critical bifurcation point is reached, it becomes impossible to incrementally determine the effective path, a total method is adopted in which the secant material stiffness is used. This secant stiffness is then reduced by a predefined factor as done in the *Sequentially Linear Approach (SLA)* developed by Rots[2] (Figure 5):

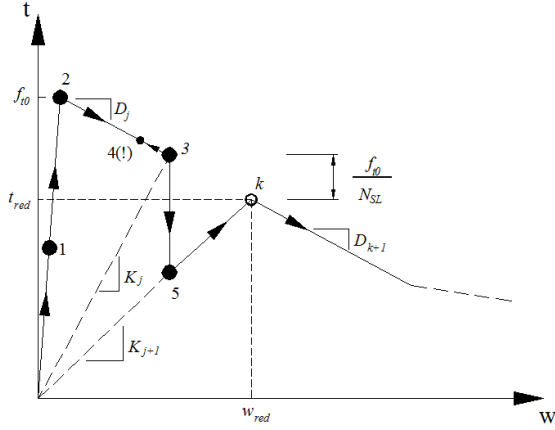


Figure 5: 1D example of the *Automatic* method

$$K_j = \frac{t_j}{w_j} \quad (4)$$

where step j is the current (valid) step and traction ‘ t ’ and displacement jumps ‘ w ’ are defined in Figure 5. In the following step $j+1$ the secant stiffness is reduced, using the standard *SLA*, such that:

$$t_{red} = t_j - \frac{f_{t0}}{N_{SL}} \quad (5)$$

where t_{red} is the new stress on the envelope, f_{t0} is the tensile strength and N_{SL} is the predefined number of *SLA* reduction steps. The next step is performed similar to the *SLA*, in which usually only one of the points will become critical and reaches the original envelope. All other points will remain on the current secant path. In the following step the incremental approach is recovered using the tangent stiffness matrix \mathbf{D} .

Note that the secant stiffness is always adopted in the total approach, which has a direct correspondence to the adopted envelope. In elastoplastic materials it is also possible to enforce the correct unloading path using the same total approach; in this case, the secant stiffness is only adopted to reach new equilibrium positions on either: i) the loading surface or ii) the unloading surface. More details can be found in [1].

2.4 Non-Iterative Energy based Method (*NIEM*)

In the *automatic* method the stepwise decrease of the secant stiffness must be

defined *a priori*, without a clear physical meaning. In order to avoid this situation a new method, designated *NIEM*, was introduced, which allows for switching between the incremental and the total approach without imposing a predefined number of reductions of the secant stiffness.

In the trial step (Figure 6), all non-critical points are treated in the usual way, such that a critical load factor λ_{crit} is computed. The goal of this step is solely to estimate the damage level that would be reached if this was a valid step; in this way, the secant stiffness update for the next step will emerge from this prediction. Nevertheless, since on step j some integration points would follow invalid paths, this step is null. The secant stiffness K_{j+1} is estimated according to:

$$K_{j+1} = \frac{t_{j+1}}{w_j + \Delta w_{trial,j}} \quad (6)$$

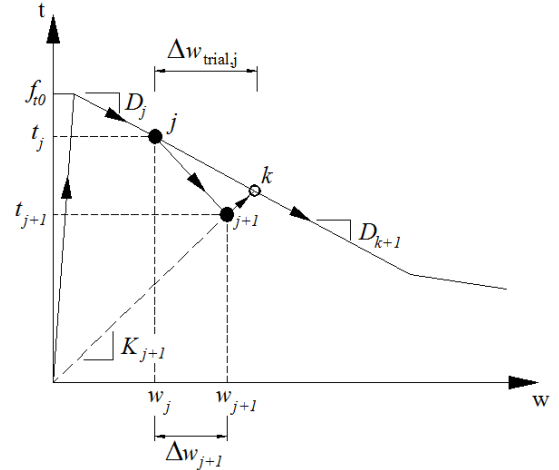


Figure 6: 1D example of the *NIEM*

Thus, in step j no change occurs; only the evaluation of the new secant stiffness is performed, which will be adopted in step $j+1$ using a total approach. In the following step the incremental approach is recovered, similar to the *automatic* method. More details can be found in [1].

3 FORMULATION FOR SOFTENING BEHAVIOUR

In the following, mode-I fracture is assumed, although adaptation for mode-II fracture is straightforward.

The modelling of non-secant unloading presents no problem in an incremental approach as long as no critical bifurcation points are attained. However, when a critical bifurcation point is found, a transition to the total approach is made. This is a consequence of the formulation presented in [1], where it was noticed that an inversion on the jump increment over the softening branch leads to an *inadmissible path*: a null step is adopted and a transition to a secant stiffness matrix occurs, similarly in both new methods.

In Figure 7, this *inadmissible path* occurs in step u , in which an unloading branch is defined between points O_u and k , with stiffness D_u . The initial stiffness D_I is assumed elastic. However, in the scope of a discrete crack approach, the initial branch usually corresponds to a penalty function. In this case, D_I is limited to an acceptable maximum value (taken as 10^3 N/mm^3 in all the examples presented). Next, the unloading stiffness D_u is defined according to:

$$D_u = (1 - d_h) D_I \quad (7)$$

where d_h is the plastic-damage scalar function ($d_h \leq d$).

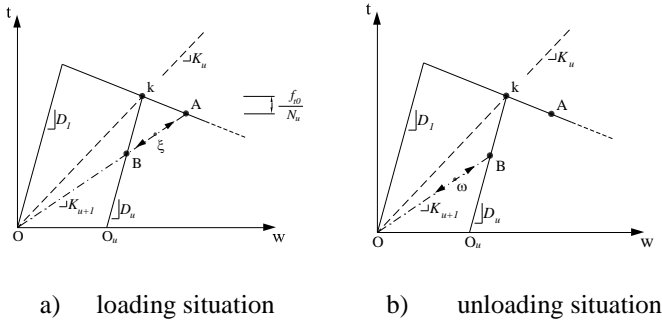


Figure 7: Softening curve: definition of the unload branch and determination of load situation

Similarly to the usual *NIEM* and *Automatic* formulations, a secant stiffness is defined for the following step. In Figure 7, the secant is defined by traction update, dividing the tensile value by N_u . This reduction parameter N_u will correspond to N_{SL} when using the *Automatic* method or a large value (say 50 to 100) when using the *NIEM*. In this way, a non-convergent cyclic behaviour is avoided. Furthermore, the

resulting increase in damage is in agreement with the experimental evidence.

In the following total step $u+1$, the previously estimated secant stiffness value is used and three situations may occur:

- i) the integration point is critical and reloads back to the envelope at point A . In this situation, in the following steps the usual incremental algorithm is followed over the original envelope;
- ii) the integration point is not critical and is positioned beyond the unloading branch (point ξ in Figure 7 a)), meaning that the effective behaviour of this integration point is *loading* and so, it will also reload back to the envelope at point A in future steps;
- iii) the integration point is not critical and lies before the unloading branch (point ω in Figure 7 b)); in this case, it is assumed that an effective unloading situation has occurred and a new envelope is generated.

The new envelope in iii) is defined by the intersection of the unloading branch with the original envelope, originating a ‘cut’ in the abscissa, eliminating the existing original surface before point k (Figure 8). In this way, the computational algorithm previously generated for the two new methods can be easily extended to the present formulation by suppressing the branches before point k and adding the *new branch*.

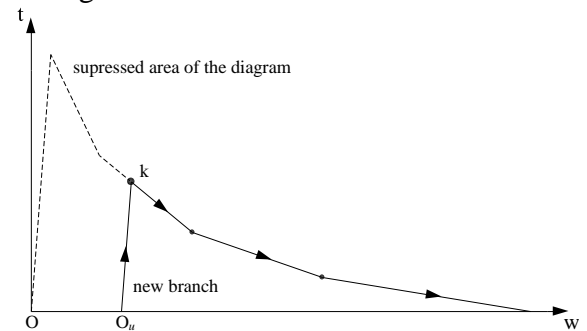


Figure 8: Softening curve: example of the insertion of an unload branch in a multilinear softening envelope

In the steps following step $u+1$, the new envelope is assumed for this integration point and several situations may develop until point k is again reached (in reloading case), either

due to the behaviour of this particular integration point alone or by influence of the remaining ones. The first situation occurs when the current state is short of (point ω in Figure 8 b)) the intersection between the current secant and the unloading branch (point B). In this case the secant stiffness is followed in both unloading and loading, in the interval between the origin O and the limit point B. If unloading to the origin occurs, crack closure is assumed; conversely, if point B is reached, a change in stiffness from k_{u+1} to D_u is adopted and the new envelope is assumed. Afterwards, when the current stress state is on the unloading branch (point ψ in Figure 9a)), the incremental approach is followed similarly to the original formulation of the method.

Loading and unloading cases are allowed on the new first branch of the transformed envelope and, in loading cases, the path will be followed incrementally until the next vertex on the linearised curve is found (Figure 9 a)) or, if an unloading situation occurs, the load factor is computed towards point O_u . In further total steps, until point k is reached, the load factor is computed such that the new envelope is aimed at the new elastic branch (point C in Figure 9 b)). The location of point C is estimated using the original *NIEM* algorithm.

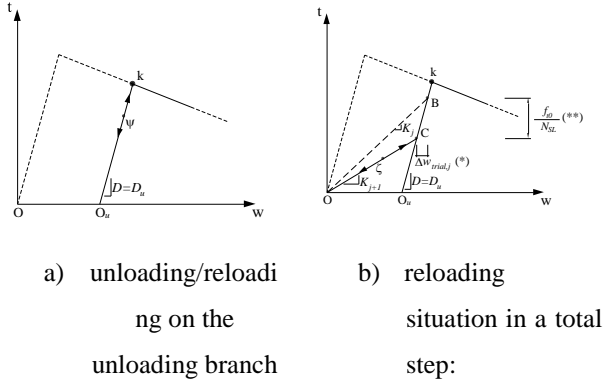


Figure 9: Softening curve: incremental/total algorithm with adapted new envelope

In the *Automatic* method the estimation of the position of point C is performed by using the usual stepwise secant stiffness update. Similarly to the first total step after this stiffness update, the secant stiffness K_{j+1} will

be followed until intersection with the unloading branch occurs.

4 DAMAGE PARAMETERS

If non-secant unloading is assumed, apart from the scalar damage value d previously, an additional parameter (d_u) is adopted. Thus, throughout the whole process the value of d is fixed, keeping the memory of the envelope stress state, whereas d_u is a temporary variable used for the definition of the secant stiffness, until full reloading is achieved. After reloading back to the envelope, d will then be normally updated with damage increase and d_u will be cleared until another unloading cycle occurs. This way, in Figure 10, the fixed damage value of the unloading point is:

$$d_k = 1 - \frac{|t_k|}{D^e |w_k|} \quad (8)$$

And, the damage of the subsequent total step will be:

$$d_{u,A} = 1 - \frac{|t_k|}{D^e |w_k + \Delta w_u|} \quad (9)$$

with, Δw_u being the jump increase due to the enforced secant update.

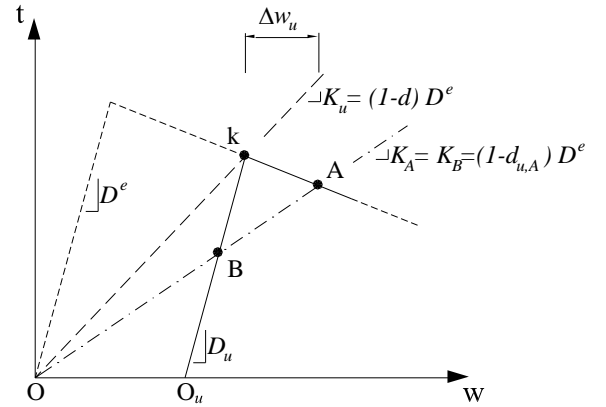


Figure 10: Softening curve: evaluation of the damage parameters

As previously stated, if there is not an effective unloading situation, the algorithm is abandoned and the original envelope will again be followed; for instance, when point A is reached, the material damage is made equal to the plastic-damage parameter at point A.

$$d = d_{u,A} \quad (10)$$

5 FORMULATION FOR HARDENING BEHAVIOUR

On Section 2, the formulation used for unloading/reloading was presented in the scope of the softening behaviour. Now, the extension to hardening behaviour is almost straightforward. First, in hardening there is no need to prevent an overestimated initial stiffness value as done in the discrete crack approach. Thus, the initial modulus D_I is the Young's modulus ($D_I = D_e$). Moreover, the secant modulus is not updated by means of stepwise stress update, but, by stepwise strain increase or stiffness reduction, which are more suitable procedures as explained in [1]. The reference points previously used in the examples are now adapted to hardening curves in Figures 11 to 14.

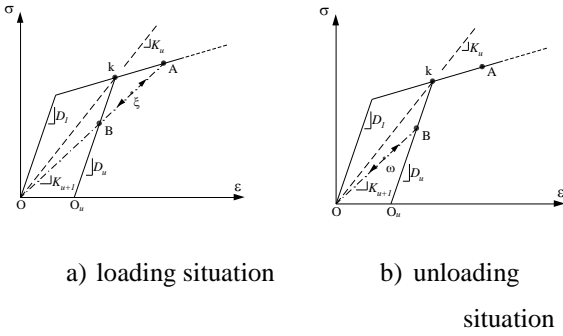


Figure 11: Hardening curve: definition of the unload branch and determination of load situation

The procedure adopted for the definition of the new envelope is similar to the previous one, supressing the area preceding point k .

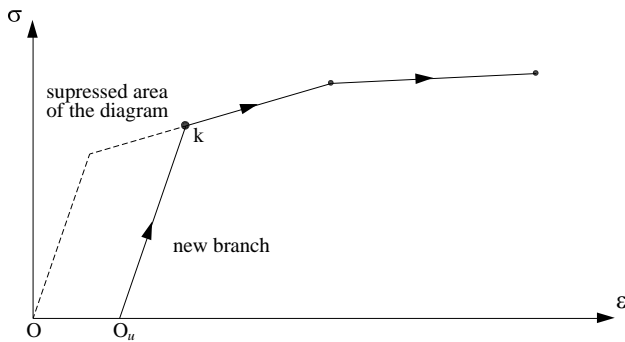


Figure 12: Hardening curve: example of the insertion of an unloading branch in a multilinear softening envelope

In Figure 13 the value $\Delta\varepsilon$ is estimated according to the additional trial step in the *NIEM*, such as implemented with softening; when using the *Automatic* method it must be evaluated by means of stepwise strain increase or stiffness reduction, obtaining the associated parameters from the linear branch.

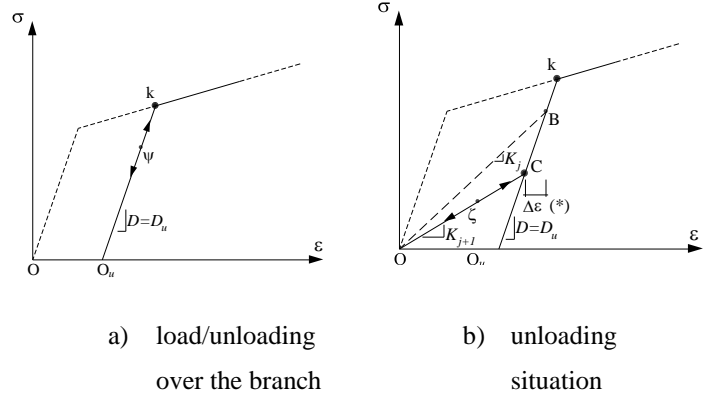


Figure 13: Hardening curve: incremental/total algorithm with adapted new envelope

Under hardening behaviour, the variable plastic-damage parameter d_u is estimated similarly to the presented before, by using the original envelope for evaluation (Figure 14). In this case, d_u is computed from the strain variation resulting from the intersection between the secant value of the current reload situation and the original envelope $\Delta\varepsilon_u$.

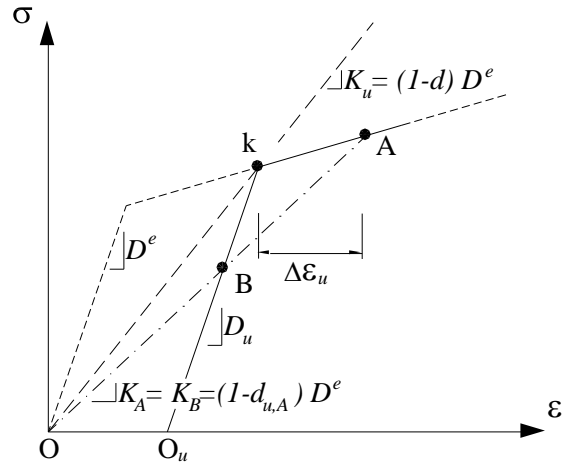


Figure 14: Hardening curve: Evaluation of the damage parameters

In Figure 15 a flowchart of the 1D algorithm is presented, where the previously reference points and indexes are used. The scheme is presented using a stress-strain

referential but it is easily converted to a traction-jump procedure.

6 STRUCTURAL EXAMPLE

In this Section, a structural example is presented in order to validate the proposed methods and discuss the different options introduced for computer analysis. Bilinear finite elements are used for the simulation of the bulk, whereas cracking is simulated using strong embedded discontinuities [5, 6]. Thus, cracks are as discontinuities embedded inside the finite parent element inserted when the tensile strength f_{t0} is attained.

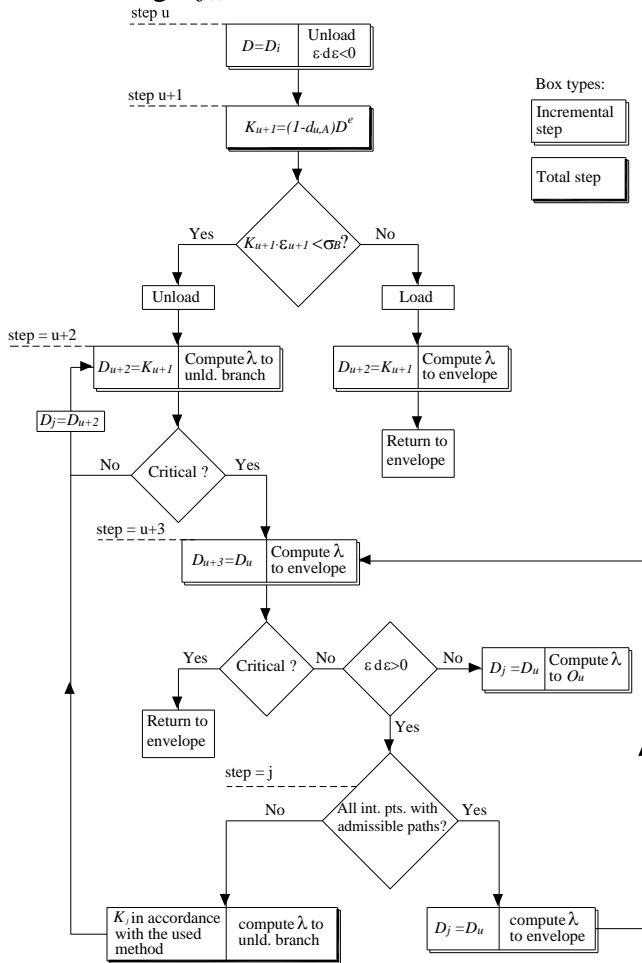


Figure 15: Flowchart with non-secant 1D unload algorithm

The displacement jumps are obtained at additional degrees of freedom, located at the embedded crack. In this model, these degrees of freedom are global, giving rise to continuous displacement jumps and tractions across element boundaries. The use of

embedded discontinuities allows for the simulation of cracking on quasi-brittle materials, with the advantage of avoiding remeshing. The use of this widespread technique has been applied to concrete in tension [6], under strong compression and to splitting failure. This type of crack simulation can also be adopted in other materials, like masonry.

As for the compressive behaviour of concrete, its modelling can become rather complex, since nonlinearities are present practically from the beginning of the loading and the material undergoes softening after peak load. Crushing is simulated using a simplified elasto-plastic model which limits the compressive stresses. It was found in previous analyses [7] that the consideration of a nonlinear pre-peak relationship does not seem particularly important on tests where concrete crushing is not the dominant failure mode. Nevertheless, the post-peak softening response may induce less bearing capacity than the assumed perfect plastic behaviour. The main reasons why the compressive softening behaviour is not adopted here are:

- i) the lack of experimental evidence, which supports the definition of a fracture energy under compression as a material parameter;
- ii) mesh size inobjectivity, which is a consequence of modelling softening within a continuum, unless regularisation approaches are used, which lie outside the scope of the present analysis.

In 2005, a study was presented with reinforced concrete beams, applying the (SLA) to models where cracking was simulated using strong embedded discontinuities. This study was summarised in [7]. These models were based on a testing campaign, and had the goal of simulating the behaviour of several experimental tests performed in reinforced concrete beams, loaded until a previously defined damage level. After this initial damage, the existing cracks were repaired by epoxy glue injection, with posterior bonding of a steel plate consisting of additional external

reinforcement. Next, the beams were subjected to additional loading until failure.

This test campaign, included the testing of a reference beam, which was loaded until failure with three unloading cycles. The aim of the present example is to illustrate the use of the unloading-reloading algorithm presented on the previous sections.

The model is a four point bending reinforced concrete beam (Figure 16) subjected to circular bending at the central span (no shear) and it is composed of concrete with $f_c = 29.67 \text{ N/mm}^2$, $f_{t0} = 2.4 \text{ N/mm}^2$, $G_{FI} = 0.056 \text{ N/mm}$. Steel reinforcement is composed of two 10 mm bars on the bottom face and two 6 mm bars on the top face. Stirrups were used on the experimental tests, but they were not modelled in the finite element mesh.

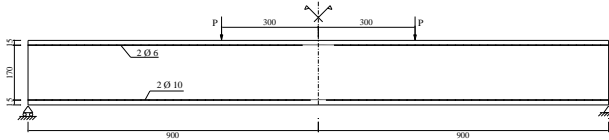


Figure 16: Unloading-reloading cycles in a reinforced concrete beam: structural scheme, load and boundary conditions (200 mm width, dimensions in mm)

The finite element model is a structured mesh (Figure 17), composed of 360 bilinear elements, with a mode-I bilinear softening law ($w_I = 0.029 \text{ mm}$ and $f_{tI} = 1.84 \text{ N/mm}^2$, $w_{ult} = 0.13 \text{ mm}$), Cracking is modelled by a discrete crack approach, using strong embedded discontinuities [5]. The traction-displacement jump relationship is characterised by a mode-I bilinear softening law; the shear stiffness is reduced proportionally to zero as mode-I softening evolves until a stress-free crack is obtained. Unloading-reloading cycles in softening are modelled by means of a linear branch with a stiffness equal to 10^3 N/mm , and the elastic stiffness in hardening.

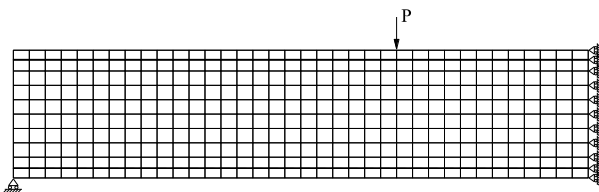


Figure 17: Unloading-reloading cycles in a reinforced concrete beam: finite element mesh

A multi-linear behaviour law for concrete under compression is adopted, which consists of the linearisation of the MC90 [8] concrete behaviour function:

$$\sigma_c = -\frac{\frac{E_{ci}}{E_{cl}} \varepsilon_c - \left(\frac{\varepsilon_c}{\varepsilon_{cl}}\right)^2}{1 + \left(\frac{E_{ci}}{E_{cl}} - 2\right) \frac{\varepsilon_c}{\varepsilon_{cl}}} f_c, \text{ for } |\varepsilon_i| < |\varepsilon_{cl}| \quad (11)$$

where:

E_{cl} is the initial tangent modulus (32000 N/mm^2);

$$E_{ci} = f_c / 0.0022;$$

ε_c is the compression strain;

$\varepsilon_{cl} = -0.0022$ is the strain value associated with f_c .

Conversely to the MC90, no softening behaviour is defined after ε_{cl} . As previously stated, this simplification is introduced in order to avoid the corresponding mesh size dependency. Thus, the adopted envelope approximates the MC90 function until the strain value ε_{cl} is attained, after which, a pure plastic behaviour is adopted (Figure 18). Unloading-reloading follows the elastic branch, parallel to the initial tangent modulus.

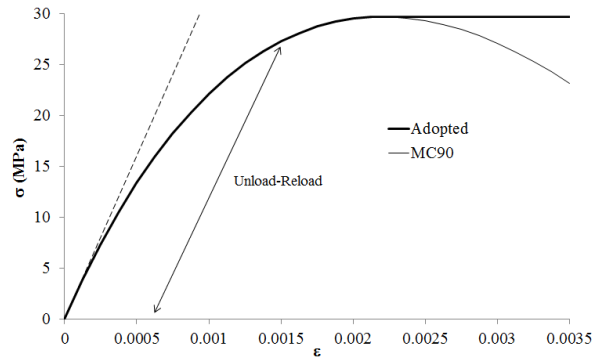


Figure 18: MC90 and adopted compression models for concrete under compression

Steel behaviour is modelled, by means of 72 Linear elements, with an elasto-plastic law ($f_y = 510.0 \text{ N/mm}^2$, $E = 205000 \text{ N/mm}^2$). The unloading-reloading stiffness is the elastic stiffness. Bond-slip is modelled using 72

interface elements under mode-II fracture, using the MC90 *local bond slip model*.

Experimentally, the beam was loaded until failure with 3 cycles; the first one until 10.0 kN, proceeded with unloading and reloaded until the second loading stage of 15.0 kN. After this second stage, the beam was unloaded and reloaded until 19.6 kN, after which the load was kept fixed for a certain period in which creep developed. Since creep is not simulated here, the plateau on the charts of Figures 19 and 20 is artificially introduced by adding the corresponding displacement.

The load-displacement curve, using the *Automatic* method, follows accurately the experimental curve, with the two first unloading branches slightly less stiff than the experimental unload-reload branches. Using the *NIEM* the curves are smoother, with similar unloading-reloading behaviour. The results of both methods do not simulate the damage increase due to the unloading-reloading loops since they were not modelled. However, the good agreement between the numerical and the experimental unloading branches and the lack of numerical difficulties opens the possibility of modelling more complex cycles.

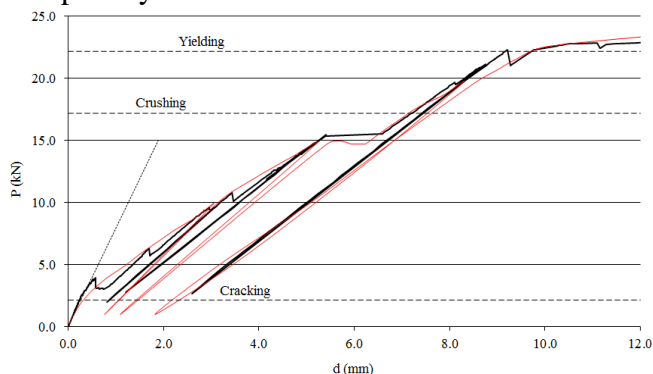


Figure 19: Unloading-reloading cycles in a reinforced concrete beam: load-displacement curve obtained using the *Automatic* method.

The deformed shapes and crack pattern are presented in Figures 21 to 23. Crack localisation is somewhat different between the methods. At failure, a diagonal crack is formed due to lack of stirrups, but the deformation limit of 12 mm prevented shear failure. On these figures the circles represent the location

of the analysed integration points presented below.

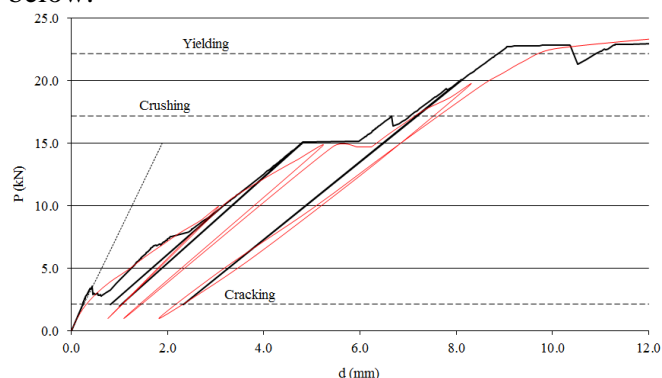


Figure 20: Unloading-reloading cycles in a reinforced concrete beam: load-displacement curve obtained using the *NIEM* method.

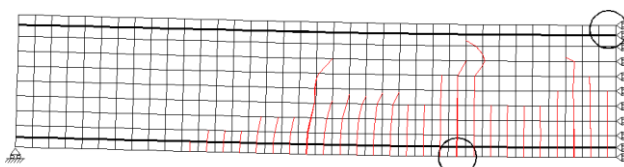


Figure 21: Unloading-reloading cycles in a reinforced concrete beam: crack superposition in the deformed finite element mesh using the *NIEM* at the initiation of the first unloading stage $\delta = 3.06$ mm (displacements amplified 5 times, crack width amplified 25 times)

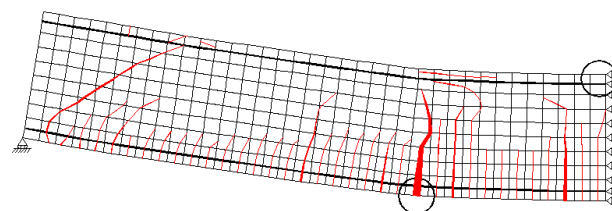


Figure 22: Unloading-reloading cycles in a reinforced concrete beam: crack superposition in the deformed finite element mesh using the *NIEM* at failure stage $\delta = 12.00$ mm (displacements amplified 5 times, crack width amplified 25 times)

In order to visualize the evolution of the concrete behaviour, the obtained stress-strain diagrams are plotted in Figure 24 for the bulk in the most compressed finite element, whereas in Figures 25 and 26 the traction-jump relations at the tip of the most opened crack are presented. For bulk compression the plotted envelope is obtained with the *NIEM*,

which is similar to the one obtained with the *Automatic* method.

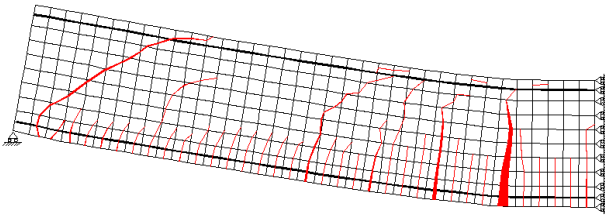


Figure 23: Unloading-reloading cycles in a reinforced concrete beam: crack superposition in the deformed finite element mesh using the *Automatic* method at failure stage $\delta = 12.00$ mm (displacements amplified 5 times, crack width amplified 25 times)

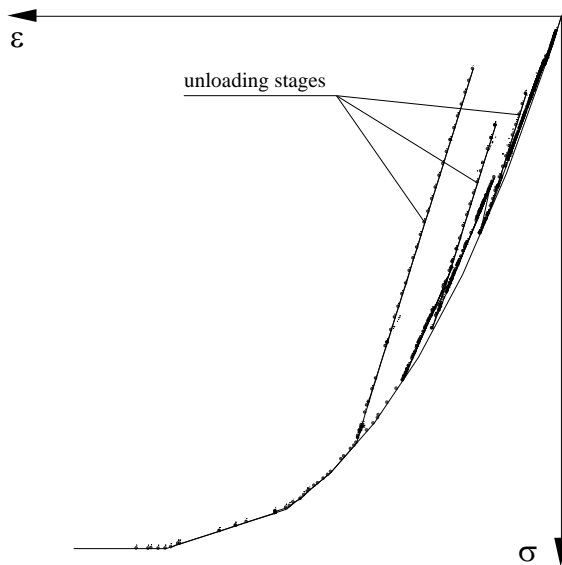


Figure 24: Unloading-reloading cycles in a reinforced concrete beam: material envelope of the most compressed concrete element using the *NIEM*.

Similarly, on the tensile softening diagrams, the unloading stages are clearly identifiable, and due to the low value of the limit traction jump, only one or two stages occur on each fracture integration points. In the cases presented in Figures 25 and 26, the last unloading stage occurred after the analysed integration reached full softening, thus, the unload steps followed the horizontal (zero stiffness) branch. The second unloading stage led to negative traction values, but no crack closure is obtained.

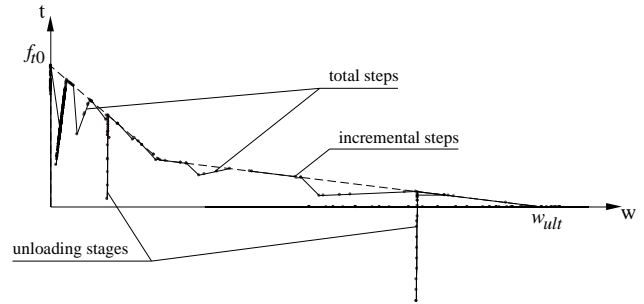


Figure 25: Unloading-reloading cycles in a reinforced concrete beam: material envelope of the most opened crack tip element using the *Automatic* method.

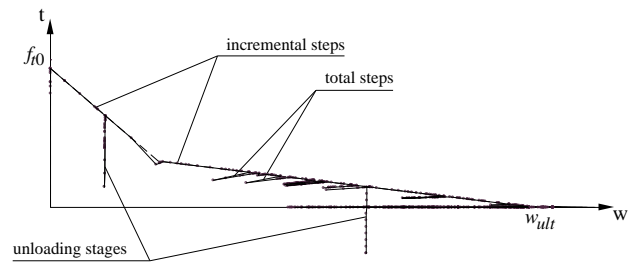


Figure 26: Unloading-reloading cycles in a reinforced concrete beam: material envelope of the most opened crack tip element using the *NIEM*.

In the steel elements Figure 27, due to the use of an elastoplastic behaviour law, the two first unloading stages occur while the elastic branch is being followed. In this way, it is only possible to visualise one unloading branch emerging from the plastic horizontal stage. Again, the envelope is naturally retrieved after reloading.

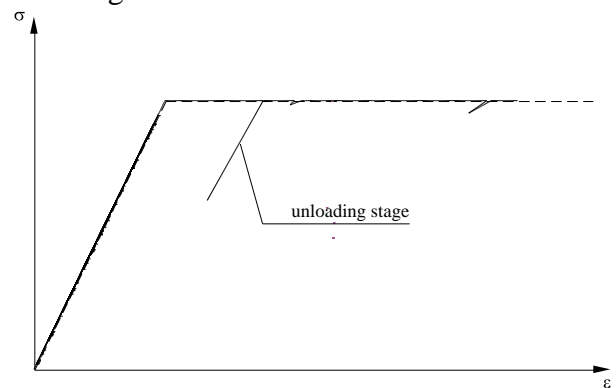


Figure 27: Unloading-reloading cycles in a reinforced concrete beam: material envelope of the most yielded steel element using the *NIEM* method.

It can be concluded that the proposed algorithm is valid and satisfactorily depicts the real unloading-reloading situations, both in hardening and in softening behaviour. Moreover, the return to the state previous to unloading is guaranteed by means of the damage variables defined in Section 3.

Since, in total steps, the material points may lay on the secant branches temporarily, before attaining the unloading/reloading branches, a softer unloading behaviour can be obtained. A new procedure is now being implemented to overcome this issue.

7 CONCLUSIONS

In models in which no critical bifurcation points arise, the following conclusions can be drawn: i) the use of an incremental approach with linearised curves has proven suitable in presented example; and ii) the energy solution control effectively allows for the correct loading path choice.

Both new methods led to good result. The *NIEM* shows a good agreement with the material laws when compared to the *Automatic* method with an acceptable increase in computing time. None of the presented methods is mesh-dependent in the scope of discrete crack approach[1].

The possibility of both methods storing the material stress/strain or traction/jump history, by means of a damage parameter, allows a perfect correlation between total (secant) and incremental (tangent) approaches, during a complete analysis, thus opening the possibility to the modelling of other type of unloading paths (other than secant), such as elastic and damage-plastic unload or even hysteretic cycles, since the coordinates of the return point on the surface are easily obtained by means of the current damage value. The presented laws, effectively model cyclic behaviour on both hardening and softening, allowing the use of a damage prediction between unloading-reloading situations. Finally, the two methods were capable of good predictions of the experimental results, conversely to the classic iterative methods which often fail to converge.

REFERENCES

- [1]. Graça-e-Costa, R., Alfaiate, J., Dias-da-Costa, D., and Sluys, L.J., A Non-iterative Approach for the Modelling of Quasi-brittle Materials. *International Journal of Fracture* (accepted), 2011. (CFRAC2011).
 - [2]. Rots, J.G., Belletti, B., and Invernizzi, S., Robust modeling of RC structures with an "event-by-event" strategy. *Engineering Fracture Mechanics*, 2008. 75(3-4): p. 590-614.
 - [3]. Graça-e-Costa, R., Alfaiate, J., Neto, P., Dias-da-Costa, D., and Sluys, L.J., Generalisation of non-iterative methods for the modelling of structures under non-proportional loading. *International Journal of Fracture* (submitted), 2012.
 - [4]. Omid, O. and Lotfi, V., Numerical analysis of cyclically loaded concrete under large tensile strains by the plastic-damage model. *International Journal of Science and Technology (Scientia Iranica)*, 2010. 17(3): p. 194-208.
 - [5]. Alfaiate, J., Simone, A., and Sluys, L.J., Non-homogeneous displacement jumps in strong embedded discontinuities. *International Journal of Solids and structures*, 2003. 40: p. 5799-5817.
 - [6]. Dias-da-Costa, D., Alfaiate, J., Sluys, L.J., and Júlio, E., Towards a generalization of a discrete strong discontinuity approach. *Computer Methods in Applied Mechanics and Engineering*, 2009. 198(47-48): p. 3670-3681.
 - [7]. Graça-e-Costa, R. and Alfaiate, J., The numerical analysis of reinforced concrete beams using embedded discontinuities. *SDHM - Structural Durability & Health Monitoring* 2006. 1: p. 11-17.
 - [8]. CEB, CEB-FIP Model Code 1990, ed. C.E.-I.d. Beton. 1991: Thomas Telford.
- Acknowledgements**
This work is supported by FEDER funds through the Operational Programme for Competitiveness Factors – COMPETE – and by Portuguese funds through FCT – Portuguese Foundation for Science and Technology under Project No. FCOMP-01-0124-FEDER-020275 (FCT ref. PTDC/ECM/119214/2010).